Energy Advances

PAPER

View Article Online
View Journal | View Issue

Cite this: *Energy Adv.*, 2024, 3, 2820

Competing effects of low salt ratio on electrochemical performance and compressive modulus of PEO-LiTFSI/LLZTO composite electrolytes†

Jiaxin Zhang,[a] Valeria Perez,[a] ThomasJae Garcia,[b] Dan-il Yoon,[a] David Wagner,‡[a] Yanika Schneider,[a] Min Hwan Lee,[b] Sang-Joon John Lee *[c] and Dahyun Oh *[a]

Polyethylene oxide (PEO)-based solid composite electrolytes (SCEs), with inorganic fillers, are studied extensively due to their effective balance between mechanical and electrochemical properties. The correlation between the composition of SCEs and their electrochemical behavior has been studied extensively, primarily focusing on the type of polymer matrix with a bias towards high lithium (Li) salt. In this study, we examine the changes in the properties of SCEs at two low EO : Li ratios, 43 : 1 and 18 : 1, in the PEO-LiTFSI matrix (with and without 10 wt% of 5 μm LLZTO) and evaluate their impact on Li stripping and plating reactions. Although higher salt concentration (18 : 1) results in substantially higher ionic conductivity (by approximately an order of magnitude), interestingly we observe that lower salt concentration (43 : 1) exhibits up to 3 times longer Li cycling life. Notably, electrolytes with low salt concentration (43 : 1) are much stiffer, with compressive modulus more than twice as high as the 18 : 1 counterpart. Although the ionic conductivity of the electrolyte is often the most immediate concern in the electrolyte design process, these findings accentuate the equal importance of mechanical properties in order to ensure successful electrolyte performance throughout prolonged Li cycling.

Received 22nd July 2024,
Accepted 27th September 2024

DOI: 10.1039/d4ya00467a

rsc.li/energy-advances

1. Introduction

As the demand for high-performance lithium-ion batteries steadily increases, there is a growing interest in safety.[1–3] Solid-state electrolytes have emerged as a promising alternative to replace conventional flammable liquid electrolytes.[4–6] However, the development of competitive solid-state electrolytes necessitates considering many factors, including high ionic conductivity, robust interfacial contact with electrodes, chemical stability, air stability, and processability.[7,8] Understanding the interplay among these factors and their impact on battery performance is essential for facilitating the integration of solid-state electrolytes into the next generation of energy storage systems. Among many different types of solid-state electrolytes, solid composite electrolytes (SCEs), a mixture of ceramics and polymers, are heavily investigated because they address most of the concerns above. Polyethylene oxide (PEO) and $Li_7La_3Zr_2O_{12}$ are widely used as a polymer matrix and ceramic filler, respectively, because of their advantages such as flexibility, good adhesion to electrodes, ease of processing (PEO), and good air stability (LLZO). In particular, combining these two components offers additional benefits when they are mixed together, enhancing mechanical flexibility, electrode contact, and ionic conductivity compared to their individual counterparts. Performance and stability have been further enhanced with dopants and co-dopants for LLZO, including tantalum,[9] aluminum,[10] niobium,[11] indium,[12] and rubidium.[13]

PEO is often selected as a polymer substrate for electrolytes because of its excellent solubility with various salts, including lithium salts, allowing it to incorporate Li ions into its polymer matrix efficiently.[14] However, PEO exhibits low ionic conductivity due to its crystallization below 60 °C.[15] Reducing the crystallinity of PEO is a common design objective to enhance ion conduction, but low crystallinity may compromise mechanical strength. Adding an air-stable ion conductor such as LLZO or LLZTO ($Li_7La_3Zr_2Ta_{0.6}O_{12}$) into the PEO-Li salt matrix has demonstrated improvements, not only in enhancing mechanical strength but

[a] Department of Chemical and Materials Engineering, San Jose State University, San Jose, California, USA. E-mail: dahyun.oh@sjsu.edu
[b] Department of Mechanical Engineering, University of California, Merced, Merced, California, USA
[c] Department of Mechanical Engineering, San Jose State University, San Jose, California, USA. E-mail: sang-joon.lee@sjsu.edu

† Electronic supplementary information (ESI) available. See DOI: https://doi.org/10.1039/d4ya00467a

‡ Present address: Department of Chemical Engineering, The University of Utah.

also in enhancing ionic conductivities, especially for high EO : Li ratio (12 : 1 or 8 : 1) matrices.[16,17] While existing studies on SCEs predominantly examine the effect of particle size, amount of particle loading, and particle surface treatment,[16–19] it is crucial to recognize that the lithium salt concentration in PEO is another important design consideration. Lowering the necessary amount of lithium salt is desirable from a practical perspective because of its high cost. Prior research in PEO-LiTFSI (lithium bis(trifluoromethanesulfonyl)imide) electrolytes has explored the effect of varying lithium salt concentrations on ionic conductivity and crystallinity, where an increase in salt concentration resulted in a decrease in the degree of crystallinity.[20,21] However, an important gap exists in our understanding of how concentrations of lithium salt change the mechanical properties of PEO-based composites electrolytes and the corresponding impact on the electrochemical reactions of Li.

In this work, we aim to bridge this gap by experimentally investigating PEO-based electrolytes at two low concentrations of lithium salt (LiTFSI, 18 : 1 (r = 0.055) *vs.* 43 : 1 (r = 0.023), (r = Li/EO[22])) with and without 10 wt% 5 μm LLZTO. We study their chemical and thermal properties using Fourier-transform infrared spectroscopy (FTIR) and differential scanning calorimetry (DSC) and also examine their behavior under macroscopic compression as well as nanoscale surface adhesion measurements by atomic force microscopy (AFM). We also determine the effect of salt concentration and LLZTO on the Li stripping and plating reaction by testing in a Li half-cell, to make a direct correlation between the compressive modulus of SCEs and electrochemical reaction with Li. The mechanical behavior of SCEs under compression holds importance in the development of high-performance solid electrolytes, especially with respect to dendrite suppression.[23] This work seeks to provide insights into both ionic transport and mechanical behavior, ultimately facilitating the design of advanced solid electrolytes tailored for practical applications.

2. Experimental

2.1. Fabrication of solid composite electrolytes

Four types of solid-state electrolytes are studied: 18 : 1 (EO : Li molar ratio) without LLZTO, 18 : 1 with 10 wt% LLZTO, 43 : 1 without LLZTO, and 43 : 1 with 10 wt% LLZTO (subsequently abbreviated as 18 : 1 no LLZTO, 18 : 1 10% LLZTO, 43 : 1 no LLZTO, and 43 : 1 10% LLZTO, respectively). The PEO-LiTFSI electrolytes were fabricated using the solvent casting method. Before the fabrication, PEO (M_v = 600 000 g mol^{-1}, Sigma-Aldrich), LiTFSI (Gotion, Inc.), and LLZTO (5 μm, Ampcera Inc.) were dried in a vacuum oven (PEO: at 40 °C for 48 h and LiTFSI/LLZTO: at 60 °C for 24 h). Anhydrous acetonitrile (ACN, Fisher Scientific, 99.8 + %) was dried for a week using molecular sieves (3 Å, baked at 350 °C for 3 hours). All electrolyte solutions used ACN as the solvent, with a weight ratio of 9 : 1 for a solvent to all solid components, including LiTFSI, PEO, and, where applicable, LLZTO. The mixtures were prepared by dissolving LiTFSI in ACN first, followed by the gradual addition of PEO and then stirred for 24 h. For samples including LLZTO, a 3 wt% of pre-dispersed LLZTO solution in ACN was added to the LiTFSI-PEO mixture and stirred for 24 h. The mixing was done inside a glovebox (MBraun Labstar, UHP Ar) and the mixture was cast onto a PTFE block using a doctor blade under N_2. The drying process involved N_2 flow at room temperature for 30 minutes, followed by vacuum drying at 65 °C for 30 minutes. The thickness of the cast electrolytes after drying ranged from 45 to 60 μm, and the films were stored in an Ar-filled glovebox and tested within one week after casting.

2.2. Electrochemical characterization

The ionic conductivity of solid-state electrolytes was measured using a potentiostat (Interface 1010E, Gamry Instruments), sweeping from 0.1 Hz to 2 MHz with 10 mV AC voltage at room temperature. The ionic conductivity of electrolytes was determined from electrochemical impedance spectroscopy (EIS) using two blocking electrodes (stainless steel discs) sandwiching the electrolyte. The ionic conductivity was calculated using the equation below.

$$\sigma = \frac{L}{R_b A}$$

where σ is the ionic conductivity in S cm^{-1}, R_b is the bulk resistance in Ω, L is the thickness of the sample electrolyte in cm, and A is the cross-sectional area in cm^2. The bulk resistance was estimated by fitting the impedance plot to an equivalent circuit model (Fig. S1B, ESI†).

Galvanostatic cycling tests were conducted with symmetric cells (Li/Electrolyte/Li) at a constant current (0.2 mA cm^{-2}) at 50 °C. The diameters of the Li disks and the electrolyte were 5 mm and 9.5 mm respectively. The electrolyte was nominally 50 μm thick, and the lithium disks were 0.75 mm thick. Linear sweep voltammetry (LSV) was performed in Li/Electrolyte/Cu cells from open circuit voltage (OCV) to 6.0 V at a scan rate of 0.1 mV s^{-1}, for which the copper foil (MTI Corp.) was 9 μm thick. The symmetric and LSV cells were assembled inside an Ar-filled glove box using a custom-designed quartz cell (Fig. S1A, ESI†), modified from a gas-tight cell in the literature.[24] After assembly, the symmetric cells were baked at 60 °C for 18 : 1 and at 65 °C for 43 : 1 for one hour. The baking temperatures were determined by the melting point using DSC.

2.3. Materials characterization

FITR spectra were collected with an iD7/iS5 (Attenuated Total Reflectance, ATR) in the 400 to 4000 cm^{-1} range. Thermal analysis was performed (total sample weight is 4–5 mg) using a differential scanning calorimeter (TA Instruments Q20) in the temperature range between 30 °C and 200 °C with a heating and cooling rate of 10 °C per minute under N_2 atmosphere. The degree of crystallinity, χ_c, for the electrolyte was calculated using the equation below.[21]

$$\chi_c = \frac{\Delta H_m}{\Delta H_{PEO} f_{PEO}}$$

where ΔH_m is the melting enthalpy of the sample in J g^{-1},

ΔH_{PEO} is the melting enthalpy of fully crystalline PEO (203 J g^{-1}),[25] and f_{PEO} is the PEO weight fraction. Optical images were collected using a high-magnification microscope (AmScope ME580TC) in transmitted-light mode. The fractional area occupied by (crystalline) spherulites was quantified by image analysis using ImageJ,[26] with detailed steps explained in the ESI.†

2.4. Macro and nanoscale mechanical characterization

Compression testing was performed with electrolytes between two 1 mm borosilicate glass slides using an ElectroPuls E1000 dynamic testing system (Instron, Norwood, Massachusetts, USA) equipped with a 250 N load cell. At the start of each test, the upper compression head was gradually lowered to a set-point of 200 mN to establish consistent minimum contact, followed by five compression cycles to 50% strain. Data were collected at a sampling rate of 100 Hz, and the continuous stress–strain curves were fitted to an exponential equation of the form $\sigma = a(e^{b\varepsilon} - 1)$. The best-fit parameters a and b were determined by minimizing the root-mean-square difference between the continuous curve and the raw data. Due to the nonlinear nature of the stress–strain data, the strain energy density, calculated as the area under the curve up to 50% strain, was used instead of Young's modulus as a scalar expression of the resistance to deformation. Force spectroscopy was performed on a commercial atomic force microscopy system (Agilent 5500 AFM) using commercial Pt-coated silicon probes (ElectricTap 150-G, BudgetSensors; spring constant of $k = \sim 5$ N m^{-1}) to measure the adhesion force between the probe and the surface of electrolytes. Samples were prepared by spin coating (2700 RPM, Instras SCK-300P) the electrolyte solution on a glass slide under N_2 (15 s for 18 : 1 and 10 s for 43 : 1) followed by vacuum-drying at 45 °C for 30 min. Each contact cycle (approach + retraction) was performed over ~6 s with a maximum contact force of ~200 nN. All nanomechanical probing was conducted in an environment chamber (~1720 cm^3) under dry nitrogen flow.

3. Results and discussion

The evolution of PEO-LiTFSI complexes in electrolytes with different salt ratios (18 : 1 and 43 : 1) was studied using FTIR (Fig. 1A). The triplet peaks (1143 cm^{-1} to 1060 cm^{-1}) associated with C–O–C stretching shared similar shapes with pure PEO in all samples, indicating that the Li concentration used in this study is relatively low.[27] The peaks corresponding to $-CH_2$ at 1466, 962, and 841 cm^{-1},[16,27] decreased as the salt concentration increased. These peaks were normalized against the one near 1109 cm^{-1} to compare their relative intensities, showing 25–42% reduced intensity of the high salt electrolyte (18 : 1) compared to the low salt electrolyte (43 : 1) (Table S1, ESI†). The normalized peak intensity at 1190 cm^{-1} corresponding to the CF_3 stretching mode of TFSI[28] increased with the high salt electrolyte, indicating the complexation of PEO with $TFSI^-$ (Table S1, ESI†).[27] The peaks at 739 cm^{-1} which originate from the CF_3 symmetric deformation of the free anion, are heightened (66–100% from low to high salt electrolyte) as salt concentrations increase,[29] (Table S1, ESI†), suggesting a higher concentration of free Li ions. However, there were no significant changes in FTIR spectra when LLZTO was introduced, indicating that LLZTO does not alter LiTFSI dissociation. Doublet peaks (1360 cm^{-1} to 1340 cm^{-1}), attributed to CH_2 asymmetric bonding, were also evident across all compositions, indicating the presence of crystalline PEO in all four solid-state electrolytes used in this study.[30] Among these doublet peaks, electrolytes with lower salt concentrations exhibited more intense peaks at 1340 cm^{-1} than those with higher salt concentrations, consistent with prior findings in PEO systems.[27,31]

The effects of LiTFSI salt concentration and inorganic fillers on the thermal behavior and the degree of crystallinity of PEO-LiTFSI electrolytes were studied using DSC (Fig. 1B, Table S2, ESI†). All of the electrolytes exhibited endothermic peaks within the temperature range of 52 °C (18 : 1) to 63 °C (43 : 1) due to the melting of PEO. Electrolytes containing higher salt concentrations (18 : 1) displayed lower melting temperatures, owing to the plasticizing effect of LiTFSI.[21] Meanwhile, the introduction of LLZTO had minimal influence on the melting temperature of the electrolytes. Fig. 1C shows the average degree of crystallinity for the different electrolytes. Overall, the crystallinity of electrolytes with lower salt concentrations (43 : 1) was higher than the high salt counterpart (18 : 1). It is generally accepted that the inorganic fillers reduce the crystallinity of PEO;[32,33] however, we observed that the inorganic fillers influence the overall crystallinity of PEO-LiTFSI electrolytes differently, depending on the salt concentrations. Adding 10 wt% of LLZTO to electrolytes with lower salt concentrations (43 : 1) led to an increase in the crystallinity, with values rising from 49% to 58%. In comparison, the impact of LLZTO on crystallinity was not evident for the higher salt concentrations (32% without, 33% with LLZTO).

While DSC revealed bulk crystallinity values, optical images were taken to examine morphological differences. In the 18 : 1 electrolyte (representative images shown in Fig. 2A and B), the spherulite boundaries exhibited more distinct contrast than in the 43 : 1 case (representative images shown in Fig. 2C and D). The corresponding binarized images are shown at the upper right inset for each case, with the interior regions of spherulites shown in black pixels and amorphous regions shown in white pixels. The 18 : 1 electrolytes exhibit less densely packed spherulites (*i.e.*, lower crystalline area fraction) than the 43 : 1 case. Comparing images of no-LLZTO images, the area fraction of spherulites (*i.e.*, proportion of crystalline regions) was 87% ± 4.6% (average ± standard deviation sampling $n = 4$ replicates for each case) for the 18 : 1 electrolytes and 93% ± 1.2% for the 43 : 1 electrolytes. The corresponding images with LLZTO particles (Fig. 2B and D) are qualitatively similar for the different salt concentrations but are not evaluated quantitatively because the particles are nonuniformly superimposed upon both crystalline and amorphous regions (along the z-axis, perpendicular to the image plane). Although limited to a 2-D imaging plane in Fig. 2, the observed larger area fraction for 43 : 1 is consistent with DSC results (Fig. 1D) that also revealed larger volumetric crystallinity for the 43 : 1 case.

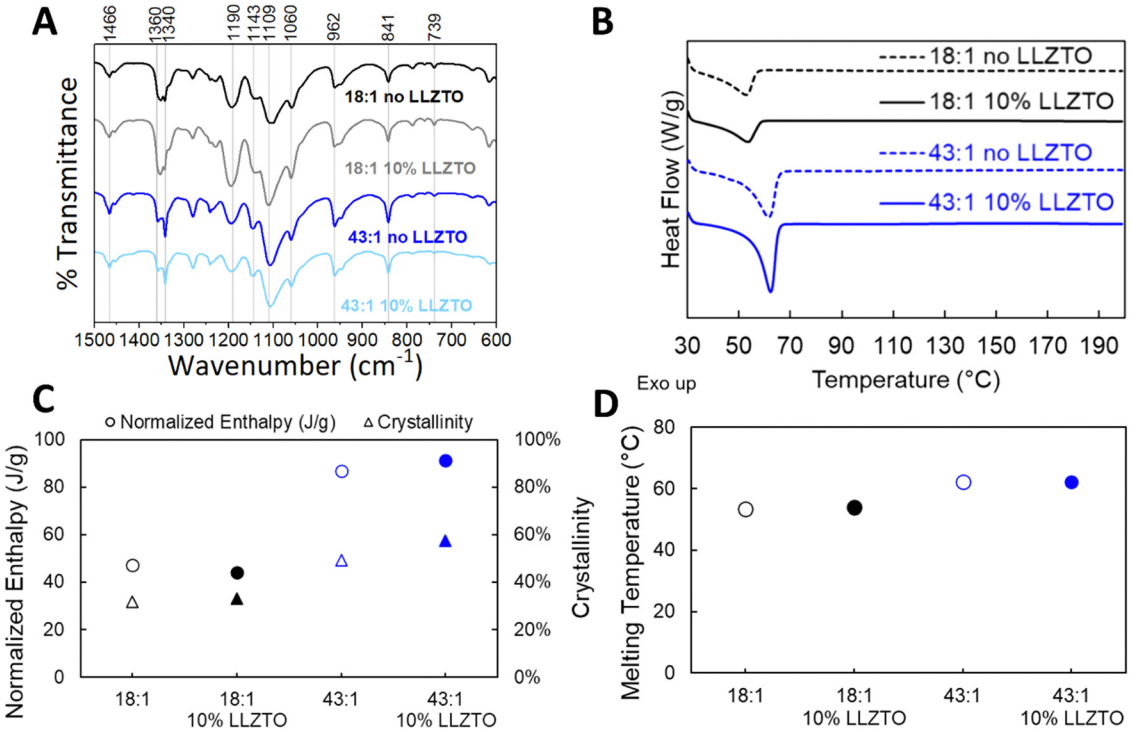

Fig. 1 (A) FTIR spectra, (B) DSC thermograms, (C) and (D) crystallinity and melting temperature plots (averaged values of two replicates) of electrolytes with varied EO : Li ratios and LLZTO content.

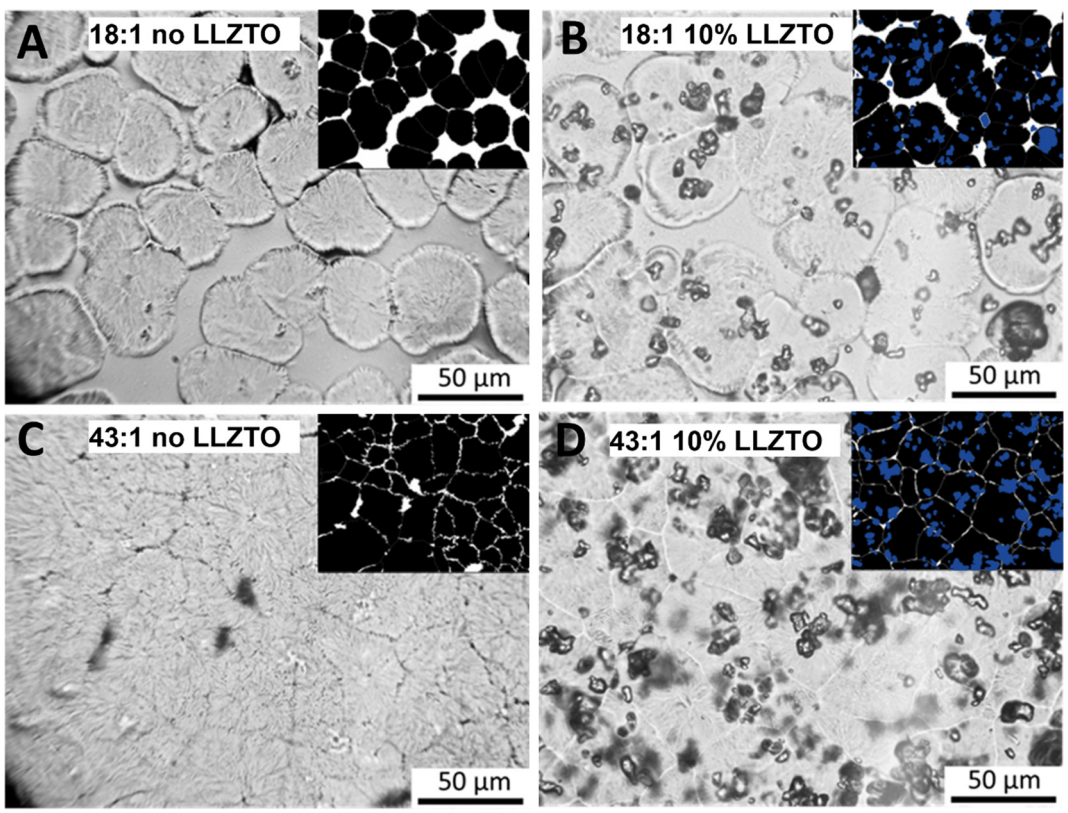

Fig. 2 Optical microscope images of solid-state electrolytes. (A) 18 : 1 no LLZTO, (B) 18 : 1 10% LLZTO, (C) 43 : 1 no LLZTO, and (D) 43 : 1 10% LLZTO. Insets of the same respective fields of view show LLZTO in blue (colors visible in digital version).

The mechanical response of the four types of electrolytes under compression was studied to understand potential implications for future use in fully assembled batteries that have confined volume (Fig. 3A). It was observed that the 18 : 1 electrolyte without LLZTO exhibited a lower compressive modulus at 0.9 kPa (computed as a linear-equivalent for strain energy density up to 50% strain) compared to the 43 : 1 electrolyte, which had a compressive modulus of 14.6 kPa. This difference in mechanical properties can be attributed to the higher proportion of amorphous regions in the 18 : 1 series, rendering them more susceptible to deformation.[34] Although both 18 : 1 electrolytes with and without LLZTO exhibited similar crystallinity, the introduction of LLZTO led to increased stiffness (9.5 times for 18 : 1 and 32% for 43 : 1) in the CPE. Among the tested electrolytes, the 43 : 1 10 wt% LLZTO composition exhibited the highest compressive modulus of 19.3 kPa, owing to its highly ordered arrangement of polymer chains and the presence of LLZTO. In contrast, the 18 : 1 10 wt% LLZTO CPE had a lower compressive modulus of 8.6 kPa.

Nanoscale indentation measurements with an AFM probe were performed to quantify differences in surface adhesion.

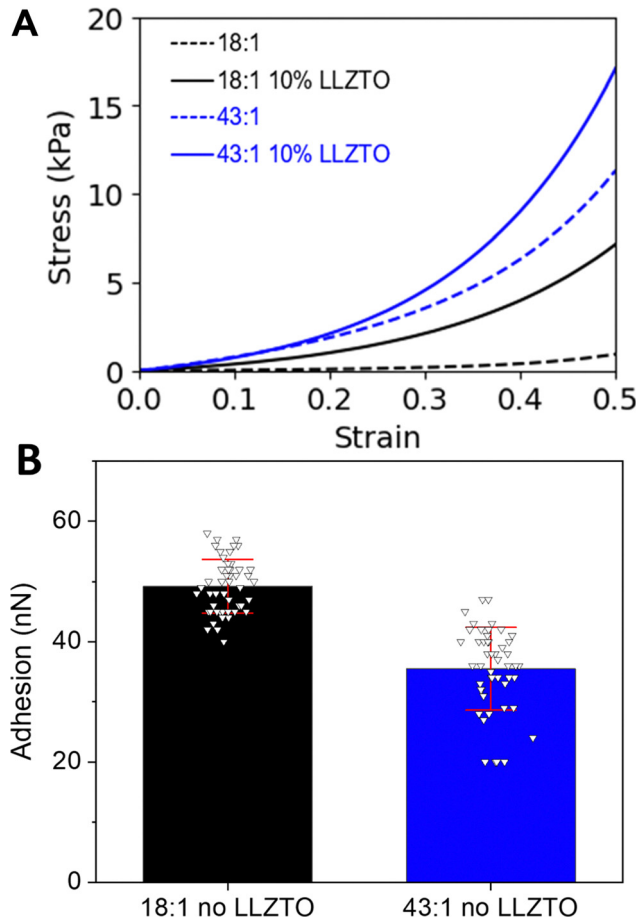

Fig. 3 (A) Fitted stress–strain curves for 18 : 1 and 43 : 1 PEO-LiTFSI electrolytes, with and without 10 wt% LLZTO wherein the fits are based on the average of two replicate data sets. (B) Surface adhesion acquired from 18 : 1 and 43 : 1 EO : Li samples by scanning probe-based force spectroscopy in dry N_2 environment.

As shown in Fig. 3B, the adhesion force between the AFM probe and sample was 49.2 ± 4.5 nN and 35.5 ± 6.9 nN (mean ± standard deviation, n = 50) for EO : Li ratios of 18 : 1 and 43 : 1, respectively. Differences appeared in measured values based on measurement location, while less variation was detected between cycles at a specific location. The observed behavior is consistent with macroscopic stress–strain behavior, in that the higher adhesion energy for the 18 : 1 case corresponds to greater compliance and, thus, higher conformality of the polymer with the indenting probe. Samples containing LLZTO were not tested with AFM due to its high surface roughness and spatial nonuniformity near and far from LLZTO particles.

Electrochemical evaluations were conducted to understand the interplay of the structural, mechanical, and surface properties in the electrochemical performance of solid electrolytes. The average ionic conductivities of 18 : 1 no LLZTO, 18 : 1 10% LLZTO, 43 : 1 no LLZTO, and 43 : 1 10% LLZTO were 6.08 × 10^{-6}, 1.98 × 10^{-6} 1.83 × 10^{-7}, and 1.51 × 10^{-7} S cm^{-1}, respectively, at room temperature. Fig. 4A shows that a higher Li salt concentration (18 : 1) increases ionic conductivity. However, large variability was observed in the higher Li salt concentration (18 : 1), which suggests poor homogeneity of the high-salt electrolytes. Furthermore, the addition of 10% LLZTO showed no beneficial effect on the ionic conductivity of both the high and low salt systems. There was a 67% reduction in ionic conductivity for 18 : 1, while a 17% reduction in ionic conductivity for 43 : 1 after adding LLZTO. We believe that the ion conduction might be partially interrupted due to the presence of LLZTO particles[35] to a greater extent for the high salt electrolyte, even though their crystallinity remains similar with and without LLZTO (based on DSC results). The decrease of ionic conductivity[34] or the increase/minimal impact on the PEO crystallinity[30] by adding the inorganic fillers were reported in other related studies for low salt containing electrolytes (less than 16 : 1 of EO : Li). The electrochemical stability windows of four electrolytes were determined using LSV measurement at room temperature (Fig. 4B). The threshold voltages are selected as the voltage at which an abrupt increase in current (*e.g.*, 3 × 10^{-7} A) is observed,[36] The corresponding values were 4.87 V, 4.79 V, 4.89 V, and 5.03 V for 18 : 1 no LLZTO, 18 : 1 10% LLZTO, 43 : 1 no LLZTO, and 43 : 1 10% LLZTO, respectively. Oxidation occurred within the range of 4.70 to 4.95 V due to the decomposition of the material. Furthermore, a reduced oxidation current was observed in the low-salt electrolytes compared to the high-salt electrolytes.

Galvanostatic cycling using half-cell tests were conducted to study the long-term effects of electrolyte properties on the Li stripping and plating behavior. Representative data for each electrolyte composition was selected from 4 to 5 replicates. We observed a sudden, significant voltage drop and fluctuating voltage profiles for both low and high modulus electrolytes when a short circuit occurred. Among the four compositions, the 43 : 1 ratio of 10% LLZTO exhibited the most stable performance up to 350 cycles, 2 to 3 times higher cycle numbers than other compositions (Fig. 4C–F). This is an interesting result because the 43 : 1 10% LLZTO electrolyte exhibited the highest

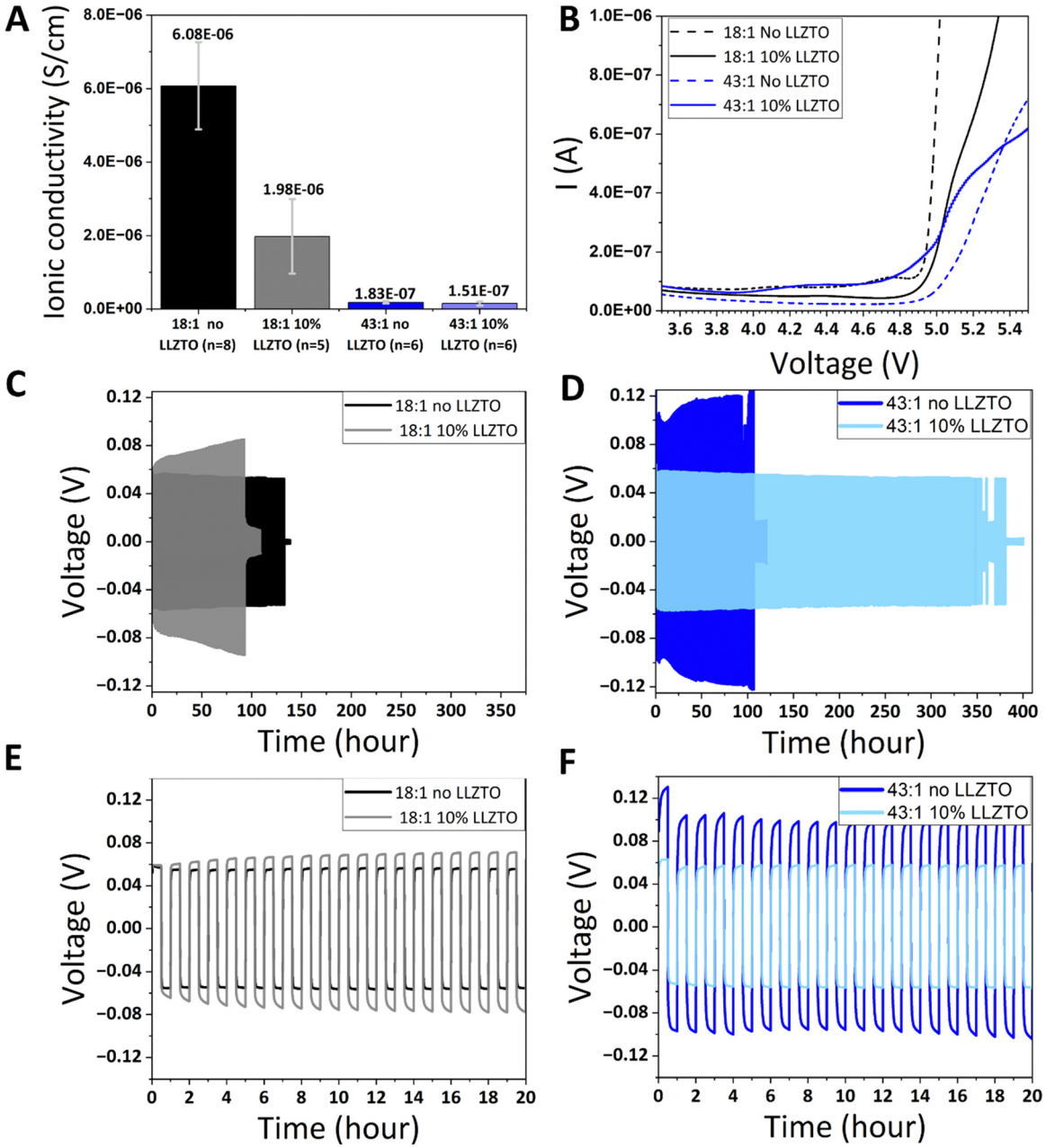

Fig. 4 (A) Ionic conductivities and (B) LSV scans (Cu/electrolyte/Li cells from OCV to 6 V) of four electrolytes at room temperature. Galvanostatic cycling of Li/electrolyte/Li symmetric cells at 0.2 mA cm^{-2} at 50 °C with high Li salt concentration (18 : 1) (C) and (E), and low Li salt concentration (43 : 1) (D) and (F) solid-state electrolytes.

compressive modulus and the lowest ionic conductivity than other compositions and the surface adhesion of the 43 : 1 electrolyte was lower than that of the 18 : 1 case. While the high salt electrolytes had higher ionic conductivities, lower crystallinity, and better surface adhesion (leading to better electrode contact), their cycling performance was poor. Solid-state electrolytes with high mechanical strength are known to be better at suppressing lithium dendrites, preventing their penetration into polymers during prolonged Li cycling.[16,17] Our findings not only accentuate the importance of mechanical properties for achieving superior Li cycling for an extended period of time, but also show the direct trade-off with respect to ionic conductivity.

4. Conclusion

In this study, we explored key factors influencing Li cycling performance, specifically Li salt concentration (18 : 1 *vs.* 43 : 1) and the use of micron-size inorganic ceramic fillers, LLZTO. We examined the chemical bonding, morphological, mechanical, and electrochemical characteristics of solid-state electrolytes.

We observed the beneficial effects of higher salt concentrations compared to lower salt concentration on ionic conductivity and surface adhesion, demonstrating a remarkable increase in ionic conductivity for 18 : 1 over 43 : 1, ranging from 13 (with LLZTO) to 33 times (without LLZTO). Additionally, there was a notable (38%) enhancement in surface adhesion at higher salt concentration. However, lower salt concentrations (43 : 1), especially in combination with LLZTO, displayed 2 to 3 times longer Li cycling life, attributed to increased crystallinity (35–43% higher than 18 : 1) and higher resistance to deformation (55% higher compressive modulus than 18 : 1) during Li cycling. In addition to its advantageous bulk properties, including a high modulus, we expect that the interfacial stability of this low-salt solid-state electrolyte can be improved by adding compounds like fluoroethylene carbonate[37,38] or lithium nitrate,[39,40] thereby enhancing lithium cycling performance. These reported trade-offs between high ionic conductivity and long-duration Li cycling emphasize the importance of salt concentration and filler particles on the optimization of material design for solid-state polymer electrolytes.

Author contributions

Jiaxin Zhang: data curation, formal analysis, resources, investigation, validation, visualization, writing – original draft, Valeria Perez: investigation, validation, visualization, writing – original draft, ThomasJae Garcia: investigation, validation, visualization, writing – original draft, Dan-il Yoon: resources, David Wagner: formal analysis, Yanika Schneider: formal analysis, Min Hwan Lee: funding acquisition, project administration, supervision, writing – review & editing, Sang-Joon John Lee and Dahyun Oh: conceptualization, funding acquisition, project administration, supervision, writing – original draft & review & editing.

Data availability

The data supporting this article have been included as part of the ESI.†

Conflicts of interest

There are no conflicts to declare.

Acknowledgements

This work was supported by the National Science Foundation (award no. 2125192 and no. 2125640) and by the Charles W. Davidson College of Engineering. The authors thank Prof. Madalyn Radlauer for support on ATR measurements.

References

1 L. Lu, X. Han, J. Li, J. Hua and M. Ouyang, *J. Power Sources*, 2013, **226**, 272–288.
2 S. Hess, M. Wohlfahrt-Mehrens and M. Wachtler, *J. Electrochem. Soc.*, 2015, **162**, A3084.
3 X. Feng, D. Ren, X. He and M. Ouyang, *Joule*, 2020, **4**, 743–770.
4 R. Chen, A. M. Nolan, J. Lu, J. Wang, X. Yu, Y. Mo, L. Chen, X. Huang and H. Li, *Joule*, 2020, **4**, 812–821.
5 P. Yao, H. Yu, Z. Ding, Y. Liu, J. Lu, M. Lavorgna, J. Wu and X. Liu, *Front. Chem.*, DOI: 10.3389/fchem.2019.00522.
6 Y. Kato, S. Hori, T. Saito, K. Suzuki, M. Hirayama, A. Mitsui, M. Yonemura, H. Iba and R. Kanno, *Nat. Energy*, 2016, **1**, 16030.
7 L. Wang, J. Li, G. Lu, W. Li, Q. Tao, C. Shi, H. Jin, G. Chen and S. Wang, *Front. Mater.*, DOI: 10.3389/fmats.2020.00111.
8 X. Chen, Z. Guan, F. Chu, Z. Xue, F. Wu and Y. Yu, *InfoMat*, 2022, **4**, e12248.
9 M. V. Reddy and S. Adams, *J. Solid State Electrochem.*, 2017, **21**, 2921–2928.
10 J. Cheng, G. Hou, Q. Chen, D. Li, K. Li, Q. Yuan, J. Wang and L. Ci, *Chem. Eng. J.*, 2022, **429**, 132343.
11 R. Wang, F. Liu, J. Duan, Y. Ren, M. Li and J. Cao, *ACS Appl. Energy Mater.*, 2021, **4**, 13912–13921.
12 Y. Teng, H. Liu, Q. Wang, Y. He, Y. Hua, C. Li and J. Bai, *J. Energy Storage*, 2024, **76**, 109784.
13 D. Hwang, M.-Y. Kim, Y.-W. Song, L. HyoChan, S.-J. Kim, B. Kang, Y. Hong, H. Kim, J. Kim and J. Lim, *Solid State Ion.*, 2023, **397**, 116245.
14 Z. Xue, D. He and X. Xie, *J. Mater. Chem. A*, 2015, **3**, 19218–19253.
15 S. Xia, X. Wu, Z. Zhang, Y. Cui and W. Liu, *Chem*, 2019, **5**, 753–785.
16 H. Zhuang, W. Ma, J. Xie, X. Liu, B. Li, Y. Jiang, S. Huang, Z. Chen and B. Zhao, *J. Alloys Compd.*, 2021, **860**, 157915.
17 F. Chen, D. Yang, W. Zha, B. Zhu, Y. Zhang, J. Li, Y. Gu, Q. Shen, L. Zhang and D. R. Sadoway, *Electrochim. Acta*, 2017, **258**, 1106–1114.
18 J. Zhang, N. Zhao, M. Zhang, Y. Li, P. K. Chu, X. Guo, Z. Di, X. Wang and H. Li, *Nano Energy*, 2016, **28**, 447–454.
19 Q. Guo, F. Xu, L. Shen, Z. Wang, J. Wang, H. He and X. Yao, *J. Power Sources*, 2021, **498**, 229934.
20 K. Pożyczka, M. Marzantowicz, J. R. Dygas and F. Krok, *Electrochim. Acta*, 2017, **227**, 127–135.
21 N. A. Stolwijk, C. Heddier, M. Reschke, M. Wiencierz, J. Bokeloh and G. Wilde, *Macromolecules*, 2013, **46**, 8580–8588.
22 L. S. Grundy, S. Fu, Z. J. Hoffman and N. P. Balsara, *Macromolecules*, 2022, **55**, 9030–9038.
23 P. Barai, K. Higa and V. Srinivasan, *Phys. Chem. Chem. Phys.*, 2017, **19**, 20493–20505.
24 B. D. McCloskey, D. S. Bethune, R. M. Shelby, G. Girishkumar and A. C. Luntz, *J. Phys. Chem. Lett.*, 2011, **2**, 1161–1166.
25 B. Wunderlich, in *Macromolecular Physics*, ed.B. Wunderlich, Academic Press, San Diego, 1980, pp. 1–127.
26 C. A. Schneider, W. S. Rasband and K. W. Eliceiri, *Nat. Methods*, 2012, **9**, 671–675.
27 S. J. Wen, T. J. Richardson, D. I. Ghantous, K. A. Striebel, P. N. Ross and E. J. Cairns, *J. Electroanal. Chem.*, 1996, **408**, 113–118.

28 I. Rey, P. Johansson, J. Lindgren, J. C. Lassègues, J. Grondin and L. Servant, *J. Phys. Chem. A*, 1998, **102**, 3249–3258.
29 L. Edman, *J. Phys. Chem. B*, 2000, **104**, 7254–7258.
30 W. Wieczorek, D. Raducha, A. Zalewska and J. R. Stevens, *J. Phys. Chem. B*, 1998, **102**, 8725–8731.
31 A. Maurel, M. Armand, S. Grugeon, B. Fleutot, C. Davoisne, H. Tortajada, M. Courty, S. Panier and L. Dupont, *J. Electrochem. Soc.*, 2020, **167**, 070536.
32 B. Kumar and L. G. Scanlon, *J. Power Sources*, 1994, **52**, 261–268.
33 L. Chen, Y. Li, S.-P. Li, L.-Z. Fan, C.-W. Nan and J. B. Goodenough, *Nano Energy*, 2018, **46**, 176–184.
34 J. Lee, T. Howell, M. Rottmayer, J. Boeckl and H. Huang, *J. Electrochem. Soc.*, 2019, **166**, A416.
35 J. Zheng and Y.-Y. Hu, *ACS Appl. Mater. Interfaces*, 2018, **10**, 4113–4120.
36 Z. Xiong, Z. Wang, W. Zhou, Q. Liu, J.-F. Wu, T.-H. Liu, C. Xu and J. Liu, *Energy Storage Mater.*, 2023, **57**, 171–179.
37 Z. Lu, J. Yu, J. Wu, M. B. Effat, S. C. T. Kwok, Y. Lyu, M. M. F. Yuen and F. Ciucci, *Energy Storage Mater.*, 2019, **18**, 311–319.
38 S. Li, G. Sun, M. He and H. Li, *ACS Appl. Mater. Interfaces*, 2022, **14**, 20962–20971.
39 Z. Zhang, J. Wang, S. Zhang, H. Ying, Z. Zhuang, F. Ma, P. Huang, T. Yang, G. Han and W.-Q. Han, *Energy Storage Mater.*, 2021, **43**, 229–237.
40 Y. Liang, W. Wu, D. Li, H. Wu, C. Gao, Z. Chen, L. Ci and J. Zhang, *Adv. Energy Mater.*, 2022, **12**, 2202493.